Journal of Applied Electrochemistry **34**: 1007–1012, 2004.

Electrochemical surface modification of aluminium sheets for application to nano-electronic devices: Anodization aluminium and electrodeposition of cobalt-copper

T. OHGAI*, X. HOFFER, L. GRAVIER and J.-Ph. ANSERMET
Institut de Physique des Nanostructures, Ecole Polytechnique Fédérale de Lausanne, CH-1015 Lausanne-EPFL, Switzerland
*(*author for correspondence, presently at: Department of Materials Science and Engineering, Nagasaki University, Bunkyocho 1-14, Nagasaki 852-8521, Japan, fax: +81 95 819 2638, e-mail: ohgai@net.nagasaki-u.ac.jp)*

Received 26 February 2004; accepted in revised form 13 May 2004

Key words: aluminium, anodization, cobalt, copper, electrodeposition, nanowire

Abstract

A nano-porous anodized aluminium oxide layer was synthesized on the surface of bulk aluminium at a wide range of anodization voltages. The barrier layer at the pore bottom of anodized aluminium oxide layer was chemically etched to make good electrical contact for nanowires electrodeposited in the pores thus formed on metallic aluminium substrates. Cathodic polarization was examined at a wide range of cathode potentials to investigate the electrodeposition behaviour of Cu and Co into the pores. $Co_{81}Cu_{19}$/Cu multilayered nanowires were fabricated using a pulse-plating technique into the templates. Co-alloy layer and Cu layer thicknesses were adjusted to 10 nm, by controlling the deposition times. The temperature dependence of the resistance of $Co_{81}Cu_{19}$/Cu multilayered nanowires grown on the template presented clean metallic characteristics and a giant magnetoresistance (GMR) of 23% was reached at 4 K.

1. Introduction

Nano-porous templates [1–3] have a variety of potential applications for the fabrication of nano-scale materials, which can be applied to functional devices with electronic, magnetic and photonic properties. Among them, magnetic nanowires are expected to the application of ultrahigh density magnetic recording medias and novel-quality magnetic field sensors. Using commercially available ion-track etched polycarbonate membrane filters, Co/Cu [4, 5] and CoNiCu/Cu [6] multilayered nanowires have been synthesized. Their magnetization and various electron transport properties were studied concerning anisotropic magnetoresistance (AMR) or current perpendicular to the plane giant magnetoresistance (CPP-GMR). The electrochemical growth of these nanowires started from a conductive metallic layer such as Au or Cu sputtered on one side of these membrane filters.

Using anodized aluminium oxide pores on the surface of metallic aluminium substrates, Ni, Co and Fe homogeneous magnetic nanowires have been also electrodeposited and characterized in terms of their magnetization properties [7–10]. Electrodeposition of Ni, Co and Fe nanowires into the 'as anodized aluminium template' can be carried out using an alternating current or a pulsed current in order to reduce the charging up effect of the barrier layer at the interface between the anodized aluminium oxide layer and the metallic aluminium substrate. However, this resistive barrier layer makes it difficult to achieve good electric contacts at the pore bottom and well-controlled layered structure of electrodeposited nanowires.

Aluminium has been conventionally used as interconnect and wiring materials in the field of microelectronics. If the template synthesis, using a *wet process* such as anodization and electrodeposition, can be directly applied to the surface of aluminium, the template synthesis will open new technological possibilities to realize low-cost processes rather than the conventional *dry process* such as e-beam and laser lithography.

In this study we report on the fabrication of anodized aluminium templates at the surface of bulk aluminium and the electrodeposition behaviour of Cu and Co into the templates. $Co_{81}Cu_{19}$/Cu mulitlayered nanowires were electrodeposited into the templates and the CPP-GMR was demonstrated. To investigate the effect of chemical etching and to confirm the electric contact at the pore bottom, the temperature dependence of the resistance was examined at low temperatures ranging downwards from 300 to 4 K.

2. Experimental details

Aluminium sheets (thickness 0.5 mm) were electrochemically polished in a solution containing 75 vol % ethanol and 25 vol % perchloric acid to achieve a mirror-like surface. The cell voltage between the aluminium anode and a gold cathode was kept at 8 V for 10 min. The polished aluminium sheets were anodized in an aqueous solution containing 0.3 mol l^{-1} oxalic acid to form a nanoporous aluminium oxide layer. To examine the anodization process, anodization voltage was varied from 10 to 90 V and the current density and the growth rate were determined. Anodized aluminium sheets were immersed in an aqueous solution containing 5 vol % phosphoric acid for 50 min to widen the pores, and to thin the oxide layer at the pore bottom. A thin gold layer (thickness 50 nm), which serves as an electrical contact for the grown nanowires, was sputtered on the surface of the template.

The electrolytic solution was prepared with ion-exchanged water containing $CoSO_4 \cdot 7H_2O$ 120 g l^{-1}, $CuSO_4 \cdot 5H_2O$ 1.6 g l^{-1}, and H_3BO_3 45 g l^{-1}. The cathodic polarization curve was measured in a wide range of cathode potential to determine the optimum conditions for Cu and Co deposition. The growth rates of the nanowires were estimated by the pore filling time, which was determined from the time-dependence of the deposition current at each potential. The electrodeposition of Co-alloy/Cu multilayered nanowires was carried out by alternating the cathode potential between −0.3 V vs Ag/AgCl (the Cu dep.) and −1.0 V (CuCo alloy dep.).

The temperature dependence of the resistance of the nanowires was measured at low temperatures downwards from 300 to 4 K using a liquid helium cryostat system. The magnetoresistance of the nanowires was measured at 300 K and 4 K using a lock-in amplifier, applying a 1 μA current and sweeping the applied magnetic field slowly up to 10 kOe(kilo-oersted, where 1 Oe = $10^3/4\pi$ A m^{-1} in SI units).

3. Results and discussion

3.1. *Anodization process of aluminium*

Figure 1(a) shows the effect of the anodization voltage on the anodization current density and (b) the growth rate of the anodized aluminium oxide layer. The anodization current density was determined by monitoring the anodization current which reaches a constant value due to a stable growth rate of the porous oxide layer. The growth rate of the anodized aluminium oxide layer was determined by the anodization time and the aluminium oxide layer thickness, which was estimated from the cross sectional SEM images of the templates. With increasing anodization voltage, the anodization current density and the growth rate of anodized aluminium oxide layer were increased exponentially as

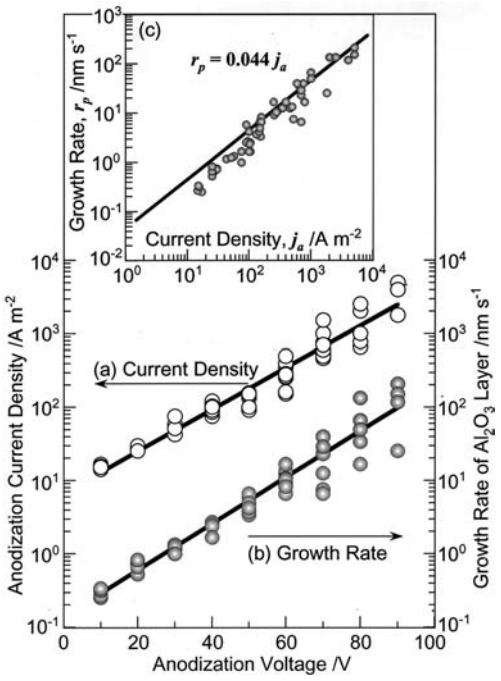

Fig. 1. Anodization current density (a) and growth rate of anodized aluminium oxide layers (b) as a function of the anodization voltage. Inset: relationship between growth rate of anodized aluminium oxide layer and anodization current density (c).

shown. This anodization current corresponds to the oxygen evolution rate (I_{oxy}) at the surface of aluminium anode and the anodization voltage contains some oxygen overvoltage (V_{oxy}), which is well known in terms of the Tafel equation, that is, $V_{oxy} = A + B \log(I_{oxy})$. According to Figure 1(a), B is around 30–40 V. This value is much larger than for insoluble anodes such as Pt and Pb in sulfuric acid. One of the reasons seems to be the existence of a resistive 'barrier layer' at the pore bottom of the anodized aluminium oxide layer. To obtain desired pore size (2000 nm length, 60 nm dia.), the optimum condition was determined to be 50 V for 10 min. Under this condition, according to Figure 1(b), the growth rate of anodized aluminium oxide film was estimated to be around 3.33 nm s^{-1}.

During anodization of aluminium, the following electrochemical and chemical reactions proceed simultaneously. One is oxygen evolution due to decomposition of water ($2\,H_2O = 4\,H^+ + O_2 + 4\,e^-$) and the other is oxidation of aluminium ($4\,Al + 3\,O_2 = 2Al_2O_3$). According to these reactions, six electrons should be provided to the anode for the production of one molecule of aluminium oxide (Al_2O_3). Therefore, the electron number: z for the above reaction is 6. According to Faraday's law, the electrochemical equivalent is described as

$$zF = M_w/\rho \tag{1}$$

Here, each parameter corresponds to the following values: faradaic constant: F = 96 485 C mol^{-1}; molecular weight

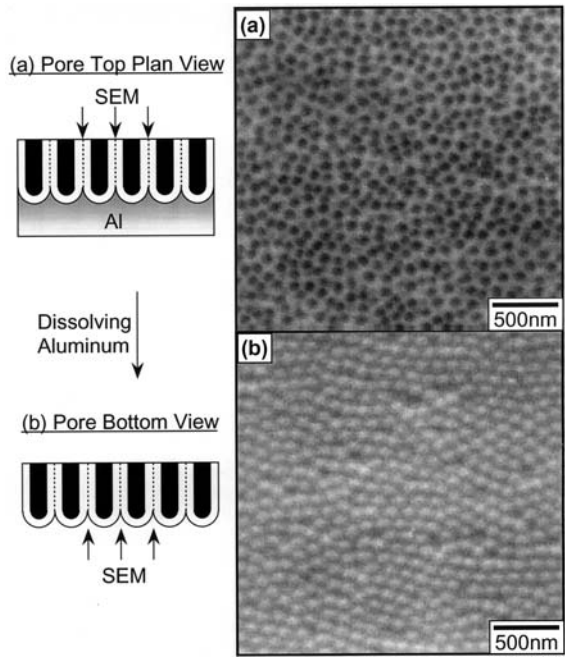

Fig. 2. SEM images of pore top plan view (a) and pore bottom plan view (b) of an anodized aluminium template. The anodization was conducted under 50 V for 10 min. The metallic aluminium substrate was dissolved in the hydrochloric acid aqueous solution containing small amount of cupric ions.

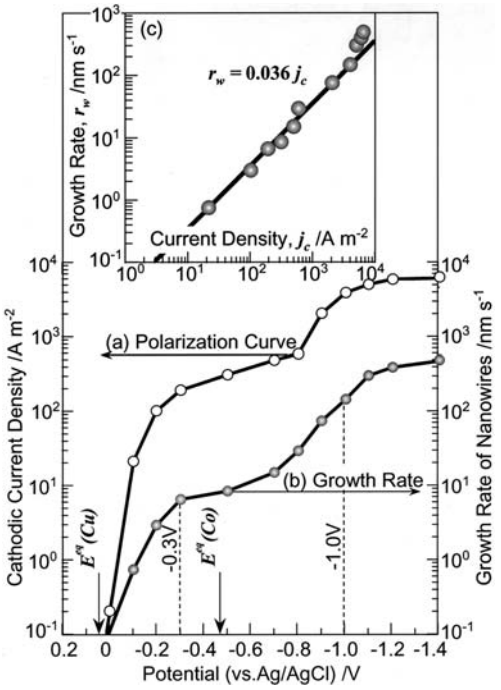

Fig. 3. Cathodic polarization curve of anodized aluminium template in the solution containing Cu^{2+} and Co^{2+} ions (a). Growth rate of CoCu nanowires at each cathode potential (b). Inset: relationship between growth rate of CoCu nanowires and cathodic current density (c). (Pore length of 2000 nm, pore diameter of 60 nm).

of $A1_2O_3$: $M_w = 101.96$ g mol^{-1}; density of $A1_2O_3$: $\rho = 4.0 \times 10^6$ g m^{-3}. Equation 1 is transformed thus:

$$r_p = 0.044 j_a \quad (2)$$

Here, r_p(nm s^{-1}) is the growth rate of $A1_2O_3$ layer and j_a/(A m^{-2}) corresponds to the anodization current density. The inset in Figure 1 shows the relationship between growth rate of aluminium oxide layer and anodization current density measured over a wide range of anodization voltages. In this Figure, the solid line was plotted using Equation 2 described in the above theoretical prediction. The experimental data corresponds well to the theoretical line at the wide range of anodization voltage (10–90 V).

Figure 2(a) shows SEM images of a pore top planar view and (b) a pore bottom back side view of an anodized aluminium template. For observation of pore bottom back side (barrier layer), the massive metallic aluminium substrate was dissolved in hydrochloric acid containing traces of cupric ions. The pore diameter is approximately 60 nm and the pore density is of the order of 10^{10} pores cm^{-2} as shown in Figure 2(a), while the oxide layer had a typical porous columnar structure and the pore length was about 2000 nm. The existence of a barrier layer is made obvious by looking at the pore bottom of anodized aluminium oxide layer (Figure 2(b)). To remove or thin this barrier layer without dissolving the metallic aluminium backing, the anodized aluminium templates were subsequently immersed in an aqueous solution containing phosphoric acid prior to the electrodeposition process.

3.2. *Electrodeposition process of cobalt and copper*

Figure 3(a) shows a cathodic polarization curve of anodized aluminium template in the solution containing Cu^{2+} and Co^{2+} ions and (b) the growth rate of electrodeposited nanowires at each cathode potential. As shown (b), the equilibrium potentials of Cu (E^{eq}_{Cu}) and Co E^{eq}_{Co} are estimated to he around +0.05 V and −0.48 V (vs Ag/AgCl) using the Nernst equation. The cathodic current occurs at the potential region close to the equilibrium potential of Cu as shown in Figure 3(a) It is well known that Cu^{2+} ions begin to electrodeposit without an accompanying overpotential from the aqua ions. Therefore, this cathodic current corresponds to the deposition current of Cu. With increasing the cathodic current, at around 100 A m^{-2}, the potential significantly polarizes to the less-noble region. This phenomenon seems to be caused by the diffusion control of Cu^{2+} ions. In the potential region less-noble than the equilibrium potential of Co, the cathodic current increases again at around −0.8 V. It is also well known that the electrodeposition of iron-group metals such as Ni, Co and Fe accompanies the overpotential [11–13] due to the rate determining multistep reduction mechanism [11]. Therefore, this cathodic current is mainly caused by the deposition current of Co. As shown in Figure 3(b), the potential dependence of the growth rate for the nanowires corresponds well to the polarization curve for Cu and Co deposition. From Figure 3, optimum conditions for the deposition potentials of Cu and Co are −0.3 V and −1.0 V (vs Ag/AgCl), that is, at potentials more noble than the diffusion control

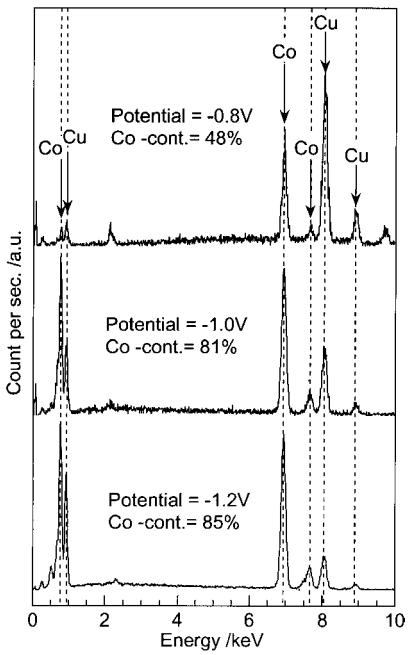

Fig. 4. Energy dispersive X-ray spectra (EDX-spectra) of CoCu nanowires electrodeposited at various cathode potentials.

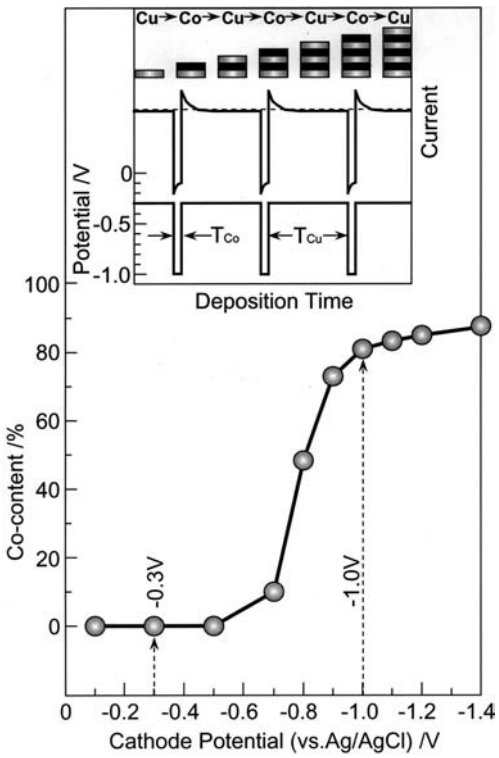

Fig. 5. Cobalt content in nanowires electrodeposited at various cathode potentials. Inset: time dependence of observed current and applied cathode potential during electrodeposition of Co/Cu multilayered nanowires.

region of each metal ions. Typical deposition rates of Cu and Co were around 10 nms^{-1} (at −0.3 V) and 20 nms^{-1}(at −1.0 V) respectively.

During the electrodeposition of nanowires, the following electrochemical reactions proceed simultaneously. One is hydrogen evolution ($2H^+ + 2e^- = H_2$) and the other is metal ion reduction ($Cu^{2+} + 2e^- = Cu$, $Co^{2+} + 2e^- = Co$). If the hydrogen evolution current is nearly zero,two electrons should be provided from the cathode for the production of one molecule of metal (Cu or Co). Therefore, the electron number: z for the above reaction is 2. Concerning the electrochemical equivalent, in Equation 1, each para meter corresponds to the following values: average molecular weight of Cu and Co: $M_w = 61.24$ g mol^{-1}; average density of Cu and Co: $\rho = 8.93 \times 10^6$ g m^{-3} Equation 1 becomes

$$r_w = 0.036 j_c \tag{3}$$

Here, r_w(nm s^{-1}) is the growth rate of nanowire and j_c(A m^{-2}) corresponds to the cathodic current density. The inset in Figure 3 shows the relationship between the growth rate of the nanowires and the cathodic current density measured in a wide range of cathode potentials. In this Figure, the solid line was plotted using Equation 3 described in the above theoretical prediction. The experimental data corresponds well to the theoretical line at the wide range of cathode potential.

Figure 4 shows the energy dispersive X-ray spectra (EDX-spectra) of CoCu nanowires electrodeposited at various cathode potentials. In these spectra, the peaks, which correspond to Cu and Co, are clearly observed at each energy levels. Using these EDX-spectra, the Co content was calculated. The samples electrodeposited at −0.8 V, −1.0 V and −1.2 V contain 48%, 81% and 85% of Co element in nanowires. Figure 5 shows Co content in nanowires electrodeposited at wide range of cathode potentials. In the potential region more noble than −0.5 V, the nanowires contain Cu only, while at the potential region less noble than −0.7 V, the Co content in nanowires increases up to around 87% with increasing cathode potential. This result corresponds well to the electrodeposition behaviour as shown in Figure 3. Consequently, $Co_{81}Cu_{19}$/Cu multilayered nanowires were electrodeposited by alternatively changing the cathode potential from −0.3 to −1.0 V as shown in the inset of Figure 5. GMR strongly depends on Co-ally layer and Cu layer thickness. When electrodeposition in pores was used, the largest values were obtained at layer thicknesses of about 10 nm [14–16]. Therefore, Co-ally and Cu layer thicknesses were adjusted to 10 nm each by controlling the deposition time at −0.3 V and −1.0 V. Typical deposition time for Cu layer and Co-ally layer were around 1.0 s (at −0.3 V) and 0.1 s (at −1.0 V). 100 bilayered $Co_{81}Cu_{19}$Cu nanowires into the templates without and with phosphoric acid etching at pore bottom were prepared for comparison.

3.3. *Magnetoresistance properties of electrodeposited Co/Cu nanowire*

Figure 6(a) shows the temperature dependence of resistance for Co/Cu multilayerd nanowires electrodeposited into the aluminium templates without and with pore bottom etching. With decreasing temperature, the resis-

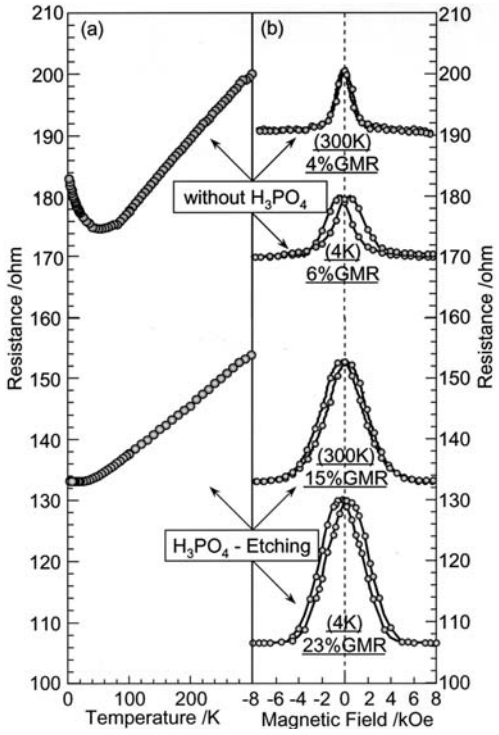

Fig. 6. Temperature dependence of the resistance (a) and the magnetoresistive hysteresis (b) of Co/Cu multilayered nanowires electrodeposited into anodized aluminium templates with and without phosphoric acid etching treatment.

tance decreases linearly in the range 100–300 K. At very low temperature less than 100 K, the resistance of samples without pore bottom etching increases with decreasing temperature, while the resistance of samples with pore bottom etching decreases with decreasing temperature. This increase of resistance at low temperature seems to be caused by the existence of a resistive barrier layer at the pore bottom, while the decrease in resistance is due to a clear metallic character. Therefore, this phosphoric acid treatment appeared to remove most or all of barrier layer at the pore bottom of aluminium template.

Figure 6(b) shows the magnetoresistive hystereses of Co/Cu multilayered nanowires electrodeposited into the templates with and without pore bottom etching. Here, the GMR ratio is defined as $\mathrm{GMR}(\%) = 100 \times R_{\max} - R_{\min})/R_{\min}$. The sample without pore bottom etching shows 4% MR ratio at 300 K and 6% MR ratio at 4 K, which is a maximum for that kind of samples. On the other hand, the sample with pore bottom etching shows 15% GMR at 300 K and 23% GMR at 4 K. With decreasing temperature from 300 to 4 K, the MR ratios increase by a factor of about 1.5, due mainly to the decrease of the minimum resistance ($R_{\min}$). It is well known that the GMR ratio depends on layer thickness, flatness of interlayer and minimum resistance. The sample without pore bottom etching has a resistive barrier layer at the pore bottom and this barrier layer causes the increasing of contact resistance. The nanowires sample with pore bottom etching have a large GMR ratio, which is almost the same value as reported previously on polycarbonate templates with gold cathode [14, 15]. Therefore, the pore bottom treatment technique using phosphoric acid successfully worked to remove most or all of the barrier layer and to make a good metallic electrical contact between aluminium substrate and electrodeposited nanowires.

4. Conclusion

The barrier layer at the pore bottom of an anodized aluminium template was chemically etched using phosphoric acid to attain a good electrical contact of electrodeposited nanowires with the aluminium substrate. $Co_{81}Cu_{19}$/Cu multilayered nanowires were fabricated in aluminium templates using a pulse-plating technique. The Co-alloy and the Cu layer thickness were adjusted to 10 nm, each by controlling the respective deposition time. The temperature dependence of the resistance for Co/Cu 100 bilayered nanowires in aluminium templates clearly showed metallic characteristics and a GMR of 23% was reached at 4 K.

Acknowledgements

This work was supported by the Swiss Commission for Technology and Innovation (CTI) through the Technology Oriented Program – Nanometer in the 21st Century, TOP-NANO21 (contract CTI no. 5812.1 TNS) and by the European Commission (EC) through the Human Potential Program – Research Training Network (HPRN), European Network on Ion Track Technology, EuNITT (contract no. HPRN-CT-2000-00047).

References

1. T.M. Whitney, J.S. Jiang, R. C. Searson and C.L. Chien, *Science* **261** (1993) 1316.
2. H. Masuda and K. Fukuda, *Science* **268** (1995) 1466.
3. T. Thurn-Albrecht, J. Schotter, G.A. Kästle, N. Emley, T. Shibauchi, L. Krusin-Elbaum, K. Guarini, C.T. Black, M.T. Tuominen and T.P. Russell, *Science* **290** (2000) 2126.
4. L. Piraux, J.M. George, J.F. Despres, C. Leroy, E. Ferain, R. Legras, K. Ounadjela and A. Fert, *Appl. Phys. Lett.* **65** (1994) 2484.
5. A. Blondel, J.P. Meier, B. Doudin and J-Ph. Ansermet, *Appl. Phys. Lett.* **65** (1994) 3019.
6. G.P. Heydon, S.R. Hoon, A.N. Farley, S.L. Tomlinson, M.S. Valera, K. Attenborough and W. Schwarzacher, *J. Phys. D: Appl. Phys.* **30** (1997) 1083.
7. D. AlMaw-lawi, N. Coombs and M. Moskovits, *J. Appl. Phys.* **70** (1991) 4421.
8. F. Li and R.M. Metzger, *J. Appl. Phys.* **81** (1997) 3806.
9. H. Zeng, M. Zheng, R. Skomski, D.J. Sellmyer, Y. Liu, L. Menon and S. Bandyopadhyay, *J. Appl. Phys.* **87** (2000) 4718.
10. A.J. Yin, J. Li, W. Jian, A.J. Bennett and J.M. Xu, *Appl. Phys. Lett* **79** (2001) 1039.
11. J. O'M. Bockris and H. Kita, *Electrochem. Soc.* **108** (1961) 676.
12. T. Tsuru, S. Kobayashi, T. Akiyama, H. Fukushima, S.K. Gogia and R. Kammel, *J. Appl. Electrochem.* **27** (1997) 209.

13. H. Nakano, K. Nakahara, S. Kawano, S. Oue, T. Akiyama and H. Fukushima, *J. Appl. Electrochem.* **32** (2002) 43.
14. B. Voegeli, A. Blondel, B. Doudin and J-Ph. Ansermet, *J. Magn. Magn. Mater.* **151** (1995) 388.
15. B. Doudin, A. Blondel and J-Ph. Ansermet, *J. Appl. Phys.* **79** (1996) 6090.
16. T. Ohgai, X. Hoffer, A. Fabian, L. Gravier and J-Ph. Ansermet, *J. Mater. Chem.* **13** (2003) 2530.